



A real-time storm surge prediction system for the Guangdong–Hong Kong–Macao Greater Bay Area under the background of typhoons: model setup and validation

Mingsen Zhou^{1,2,3} · Chunxia Liu^{1,2,3} · Guangfeng Dai¹ · Huijun Huang^{1,2,3}  · Qingtao Song^{1,2,3} · Mengjie Li¹

Received: 14 March 2024 / Accepted: 20 September 2024
© The Author(s), under exclusive licence to Springer Nature B.V. 2024

Abstract

Storm surges are the most severe type of marine disaster affecting the Guangdong–Hong Kong–Macao Greater Bay Area (GBA), and storm surge forecasting under the background of typhoons remains challenging. In this paper, we propose an operational coupling model (including the global–regional assimilation and prediction system [GRAPES] atmospheric model and the finite volume coastal ocean model [FVCOM]) to predict typhoon-induced storm surges in the GBA, namely, the Greater Bay Area Storm Surge Prediction System (GBASSP), and verified its performance. The highest horizontal resolution of the GBASSP is 80 m, and it has the following advantages. (i) It can provide early warning and forecasting for storm surge at least 2 days before typhoon landfall. (ii) For the next 24-hour forecast of a single typhoon, the maximum storm surge error is only 5 cm, while the mean absolute error of the maximum storm surge of the GBASSP is 19.7 cm. The difference in the occurrence time of the maximum storm surge between observations and the GBASSP is within 1 h. (iii) Comprehensively compared to other storm surge prediction models, the GBASSP performs well and has the best forecasting skills. The relative and root mean square errors of the GBASSP are 5.9% and 21 cm, respectively, the smallest of all the comparative models used in this study. In addition, the average absolute error is between those of the other models.

Keywords Storm surge · Prediction · Guangdong–Hong Kong–Macao Greater Bay Area · FVCOM · GRAPES

✉ Huijun Huang
hjhuang@gd121.cn

¹ Guangzhou Institute of Tropical and Marine Meteorology, Guangdong Provincial Key Laboratory of Regional Numerical Weather Prediction, China Meteorological Administration, Guangzhou 510080, China

² Guangdong Provincial Marine Meteorology Science Data Center, Guangzhou 510080, China

³ Dianbai National Climate Observatory, Maoming 525400, China

1 Introduction

Storm surge refers to the phenomenon of abnormal sea level rise caused by strong atmospheric disturbances, such as tropical cyclones (TCs) and extratropical cyclones (Needham et al. 2015; Salmun and Molod 2015; Muis et al. 2016; Kohno et al. 2018; Tadesse et al. 2020), but storm surges are also modulated by the coastal bathymetry (Pore 1964; Cochran et al. 2019). Storm surge disasters rank first among marine disasters, and most of the extreme coastal disasters caused by typhoons around the world are caused by storm surges (Petzelberger 2000; Von Storch and Woth 2008; Needham et al. 2015; Kohno et al. 2018). Needham et al. (2015) pointed out that storm surges are among the most deadly and costly global catastrophes. The most severe surge events have killed hundreds of thousands of people and caused extraordinary economic losses across the globe, including Hurricane Katrina in 2005, Hurricane Sandy in 2012 in the United States, and Cyclone Nargis in 2008 in Myanmar. According to the Bulletin of China Marine Disaster (2020–2021), storm surge disasters are the most serious of all types of marine disasters regarding economic losses, accounting for 97% of the total direct economic losses (Guo et al. 2022).

Storm surge forecasting remains challenging (Needham et al. 2015; Kohno et al. 2018; Cochran et al. 2019). Research on storm surge forecasting has been conducted for a long time. Research has developed rapidly from the early probabilistic statistical method to the current numerical prediction method. Currently, two main storm surge prediction methods exist: empirical statistical and numerical prediction. Currently, the primary technique of storm surge forecasting is based on a numerical prediction model. This type of model was developed many years ago (Jelesnianski 1972; Banks 1974; Greenberg 1977; Henry 1982; Gray et al. 1984), and there has been slight recent improvement in the physical processes (Kohno et al. 2018). The improvement has mainly been carried out in dynamic aspects such as the grid resolution or coordinates (Sasaki and Iizuka 2007; Kohno et al. 2018; Bloemendaal et al. 2019). Physical understanding of storm surges and prediction models has matured in this sense. The latest improvements focus on the dynamic framework of the model, e.g., unstructured methods. For example, the finite element method (FEM) or finite volume method (FVM), advanced circulation (ADCIRC) model (Luettich and Westerink 2004), semi-implicit Eulerian-Lagrangian finite element (SELF) model (Zhang and Baptista 2008), and Delft3D (Deltares 2014) are becoming popular (Kohno et al. 2018).

The unstructured grid, employed to perform coastal numerical models with a high resolution, is a new trend for improving the accuracy of storm surge simulations. More and more FVM models are being developed to predict coastal storm surges around the world (Chen et al. 2003; Fringer et al. 2006; Zhang et al. 2016, 2021; Kohno et al. 2018; Androsov et al. 2019). For example, concerning the coastal areas across the entirety of China, a high-resolution typhoon storm surge model (based on the ADCIRC model) developed by Liu et al. (2014) has a maximum horizontal resolution of 300 m and has an adequate calculation accuracy and efficiency for future operational running. Feng et al. (2016) used the ADCIRC model and simulating waves nearshore (SWAN) wave model to establish a refined storm surge model for southeastern China with a maximum horizontal resolution of 100 m in Fujian Province. Based on their test, they found that the model runs fast enough to meet operational requirements when more computational cores are used. By coupling the National Center for Environmental Prediction-climate forecast system reanalysis (NCEP-CFSR) model and the finite volume coastal ocean model (FVCOM), Chu et al. (2019)

developed a storm surge model with a resolution of 0.5–20 km for the East China Sea. Their study found that the best forcing and drag coefficient combination can generally improve storm surge models' performance. Zhang et al. (2021) established a storm surge model for the coastal city of Ningbo by coupling the Holland wind model and the ADCIRC model. Its highest resolution is 5–10 m, and the storm surge and total tide level are well simulated. It should be noted that while the results of the simulations of these models are accurate, the systems they build are either inadequate in resolution (≥ 300 m) or experimental (it is not an operational prediction system).

The Guangdong–Hong Kong–Macao Greater Bay Area (GBA) is an urban agglomeration of nine cities (Guangzhou, Shenzhen, Zhuhai, Foshan, Dongguan, Zhongshan, Jiangmen, Huizhou, and Zhaoqing) and China's special administrative regions of Hong Kong and Macao (Fig. 1). It is the most developed area in Guangdong Province, and the average direct economic losses caused by storm surges in the past ten years are approximately \$2.6 billion RMB (Bulletin of China Marine Disaster, 2022). This area has experienced rapid population and economic growth since the 1980s. With a growth rate of 4.5% per year, by 2010, the GBA megacity surpassed Tokyo as the world's largest urban area in both size and population (World Bank et al., 2015), and the total number of inhabitants is currently greater than 80 million. The GBA's gross domestic product (GDP) exceeds US \$1 trillion,

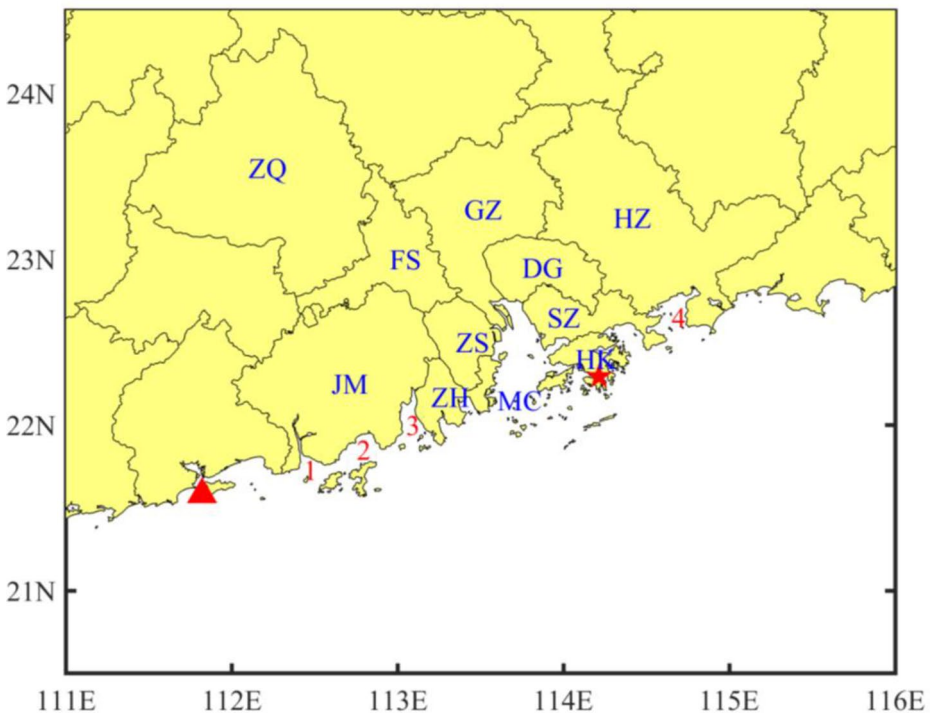


Fig. 1 Cites in the Guangdong–Hong Kong–Macao Greater Bay Area (GBA), including Zhao Qing (ZQ), Guang Zhou (GZ), Hui Zhou (HZ), Fo Shan (FS), Dong Guan (DG), Jiang Men (JM), Zhong Shan (ZS), Shen Zhen (SZ), Zhu Hai (ZH), Macau (MC), and Hong Kong (HK). The red star indicates the location of the observed water level station, Quarry Bay, and the red triangle indicates the location of the Zhapo observed water level station. Number 1 is the location of Zhenhai Bay, 2 is the location of Guanghai Bay, 3 is the location of the Huangmao Sea, and 4 is the location of Daya Bay

placing it among the top 20 national economies worldwide (International Monetary Fund 2018). However, it is a low-lying flood-prone coastal area and is affected by sea level rise and the extreme water levels caused by storms (He et al. 2014; Huang et al. 2004; Li et al. 2018; Qu et al. 2018; Yang et al. 2015; De Dominicis et al. 2020). Hallegatte et al. (2013) predicted that estimated flood losses for Guangzhou would exceed U.S. \$13 billion by 2050 under the scenario of a relative sea level rise of 0.6 m and with adaptation to maintain the present flood probability.

Storm surges induced by TCs cause significant damage in bay areas (Takagi et al. 2014; Needham et al. 2015; Oey 2016; Choy et al. 2020; Shi et al. 2020). Severe disasters caused by storm surges still occur worldwide (Table 1). Considering the number of cases, it is clear that significant storm surge disasters arise infrequently, but their impact can be severe when they occur. For example, Super Typhoon Mangkhut (1822) made landfall on the coast of Jiangmen City in China. It swept across Guangdong, killed five people, impacted over three

Table 1 Major storm surge disasters in recent years and the coupled model forecasting technology*

TC	Year	Maximum intensity	Affected area	Economic losses (billion)	Fatalities	Typical storm surge	Coupled model forecasting technology**
Katrina	2007	902 hPa	Gulf of Mexico	\$108	1,833	4–7 m	Atmosphere: Typhoon parameter Ocean: polar grid, two-dimensional (Jelesnianski et al. 1984)
Sidr	2007	944 hPa	Bay of Bengal	\$1.7	~15,000	3–6 m	Not Found
Nargis	2008	962 hPa	Bay of Bengal	\$12.9	138,366	3–5 m	Not Found
Sandy	2012	940 hPa	East Coast of USA	\$68	233	~4 m	Atmosphere: Typhoon parameter Ocean: polar grid, two-dimensional (Jelesnianski et al. 1984)
Haiyan	2013	895 hPa	Beibu Gulf	\$2.86	7,403	5–7 m	Atmosphere: Typhoon parameter Ocean: two-dimensional (Kohno et al. 2018)
Winston	2016	884 hPa	Fiji	\$1.4	44	~3 m	Atmosphere: Typhoon parameter Ocean: two-dimensional (Kohno et al. 2018)
Irma	2017	914 hPa	Caribbean Islands	>\$64.76	146	3–4.5 m	Atmosphere: Typhoon parameter Ocean: polar grid, two-dimensional (Jelesnianski et al. 1984)
Hato	2017	935 hPa	GBA	\$6.82	24	3–4 m	Atmosphere: Numerical forecast wind Ocean: unstructured grid, three-dimensional***
Mangkhut	2018	910 hPa	GBA	\$1.95	5	3–4 m	Atmosphere: Numerical forecast wind Ocean: unstructured grid, three-dimensional***

*All data on economic losses and fatalities are from Kohno et al. (2018), except for those on the economic losses and fatalities of Typhon Mangkhut, which come from Choy et al. (2020). ** All of the coupled models presented here are unidirectional. ***The forecasting technology used in this paper

million people, forced the evacuation of 1,600,000 people, and caused economic losses of approximately 14.5 billion RMB in China (Choy et al. 2020). During Typhoon Mangkhut, the storm surge increased significantly, the submergence lasted long, and the increased water carried a large amount of sediment ashore. Typhoon Mangkhut caused the most significant storm surge of 183–339 cm at the water level stations in the Pearl River Estuary (PRE). The extensive damage caused by Super Typhoon Mangkhut prompted this study.

Previous researchers have been working hard to develop storm surge forecasting technology based on an air-sea coupling model. Since the 1980s, the Sea Lake and Overland Surges from Hurricanes (SLOSH) model (Jelesnianski et al. 1984) has been predominantly employed for forecasting storm surges (such as during hurricanes Katrina, Sandy, and Irma) in North America. This model is a polar grid, two-dimensional storm surge model forced with a typhoon parameter hurricane wind model (e.g., the Holland model (Holland 1980)). This model has rapid computation times because it does not require output from atmospheric model computations. For typhoons Haiyan and Winston, the storm surge information is available from the World Meteorological Organization (WMO) Storm Surge Watch Scheme provided by different Regional Specialized Meteorological Centers (RSMCs). Moreover, in the North Indian Ocean, RSMC-Delhi began issuing storm surge graphical advisories in 2009, while RSMC-Nadi (Fiji Meteorological Service, FMS) plans to issue real-time storm surge guidance in the South Pacific region in the near future (Kohno et al. 2018). Herein, we propose an operational coupling model to forecast storm surges in the GBA. The atmospheric model in our coupled model is now a more popular and precise numerical forecasting model, and the oceanic model has an unstructured grid that better represents the complex topography in a coastal region.

To forecast storm surges in the GBA, we coupled an unstructured grid, three-dimensional hydrodynamic model (the FVCOM model) developed by Chen et al. (2003) with the global-regional assimilation prediction system (GRAPES) atmospheric model.

In this study, we focused on establishing a real-time storm surge prediction model for the GBA, namely, the Greater Bay Area storm surge prediction system (GBASSP), and we validated the results of our model for recent TCs. Many studies have shown that there are strong interactions between typhoons and the ocean at various spatiotemporal scales (Emanuel et al., 1986; Sriviver and Huber 2007; Jin et al. 2014; Huang et al. 2015; Zhou et al. 2019). Using the GBASSP model we established, we predicted and validated the storm surges caused by strong typhoons and those caused by weak typhoons in recent years. Our results showed that the maximum storm surge and prediction error for weak typhoons were smaller than those for strong typhoons. However, to best represent the typhoons that affected the GBA and to compare our predictions with other models, only the results of strong typhoons are discussed in this paper. The remainder of this paper is organized as follows: Sect. 2 describes the data and methods used in this study. Section 3 presents the prediction performance of the GBASSP. Section 4 presents the warning capability of the model. Section 5 presents the discussion and main conclusions.

2 Model, data, and methods

2.1 Model

This section describes the composition and configuration of the GBASSP. Figure 2 presents a flowchart of the processing steps of the newly developed GBASSP model. The GBASSP consists of an oceanic model (FVCOM) and an atmospheric model (hereafter GRAPES-3 km), and it is unidirectionally coupled, with the atmospheric model transmitting 10-m wind and sea-level pressure data to the ocean model every hour. It runs twice daily (00:00 UTC and 12:00 UTC; all of the times in this paper are UTC if not specified) and provides hour-by-hour forecasts for the next 3 days. When it starts, the first step is pre-processing. In this step, the FVCOM (1) prepares a dry/wet grid, terrain, and bathymetric data file; (2) uses the data from step (1) to process the model grid and interpolate the bathymetry, and (3) generates the input files, e.g., a grid file and open boundary tidal file. The GRAPES-3 km model (1) prepares the initial field, (2) sets the model grid and interpolates the wind and air pressure to the model grid, and (3) generates the driving files for the FVCOM. The second step of the GBASSP is running the FVCOM main program, and the third step is post-processing. In the third step, the model produces information about the storm surge, such as the water level at each forecast time and the times series of the forecast storm surge at Zhapo/Quarry Bay station. The last step is to issue early warning information according to the post-processing results.

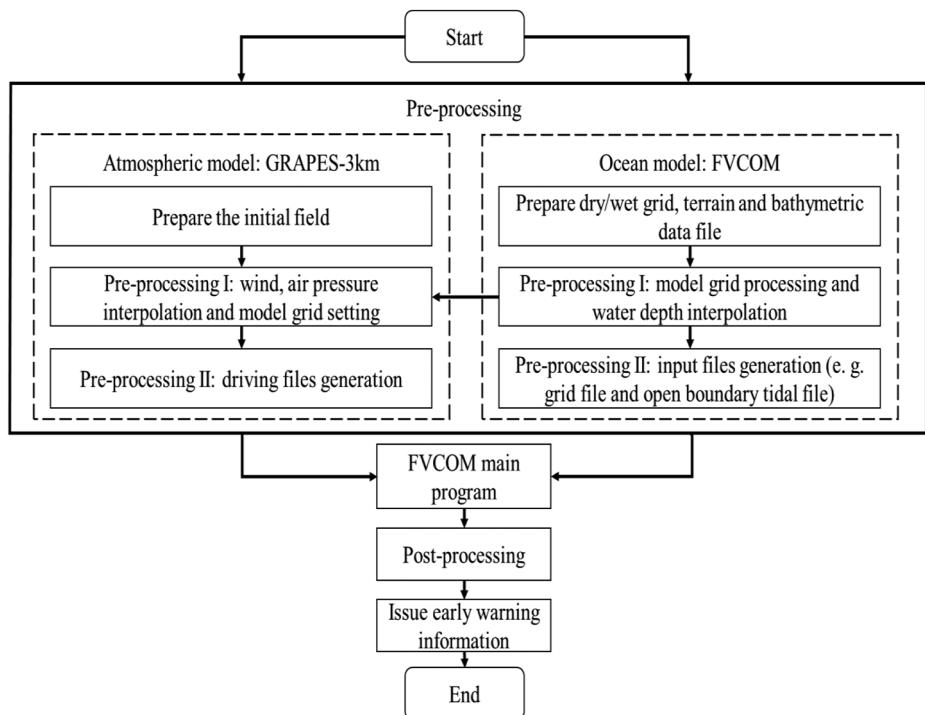


Fig. 2 Flowchart of the Guangdong–Hong Kong–Macao Greater Bay Area storm surge prediction model (GBASSP)

Currently, the time from the start of the system to the end of the main program of the model is ~70 min when 480 computational cores are used. Through the post-processing, the results are shown on the website after another 30 min. The model is fast enough to meet operational requirements. The system can run faster when more computational cores are used. We tested the model and determined that when 960 computational cores are used, the time is reduced to 45 min. In the near future, the runtime of the GBASSP is expected to be reduced to half of what it is today. The forecast results can be seen at <http://10.148.8.18/ywwhome/vision/home.jsp>. Because the system is currently only used on a small scale (such as by government departments and meteorological bureaus), the website can only be accessed through specific IP addresses.

2.1.1 Oceanic model (FVCOM)

As shown in Fig. 2, the ocean model of the GBASSP is FVCOM. It is an unstructured grid, finite-volume, three-dimensional primitive equation coastal ocean model jointly developed by the University of Massachusetts-Dartmouth and the Woods Hole Oceanographic Institute (Chen et al. 2003). It provides a better representation of the mass, momentum, and heat conservation laws in a coastal region with complex geometry, as well as a better simulation of tidal elevations and residual currents, especially around islands, barriers, and inlets with complex topography (Chen et al. 2003). It is cast in a generalized terrain-following coordinate system in the vertical direction and the control volumes of unstructured triangular meshes in the horizontal direction. The spatial fluxes of the momentum are discretized using a second-order accurate finite-volume method (Kobayashi et al. 1999). The diffusion and mixing parameterizations used in the FVCOM are the Smagorinsky scheme (Smagorinsky 1963) in the horizontal direction and the General Ocean Turbulence Model (Burchard 2002) in the vertical direction, and the 2.5-level Mellor-Yamada (Mellor and Yamada 1982) turbulence model is used as the default. Although FVCOM has a river module, we do not consider the effect of river discharge on water level due to a lack of river discharge data.

The bottom friction stress is calculated using the following equation:

$$(\tau_{bx}, \tau_{by}) = C_b \rho_w (u_b, v_b) \sqrt{u_b^2 + v_b^2} \tag{1}$$

Where (u_b, v_b) represents the x and y components of the bottom current velocity, and the bottom drag coefficient C_b is determined by matching a logarithmic bottom layer to the model at a height Z_{ab} above the bottom, which can be mathematically expressed as:

$$C_b = \max \left(\frac{k^2}{\ln \left(\frac{Z_{ab}}{Z_0} \right)^2}, 0.0025 \right) \tag{2}$$

Where $k = 0.4$ is the von Karman constant and Z_0 is the bottom roughness parameter.

Wind stress is computed using the conventional formulation with respect to the wind speed, as follows:

$$\vec{\tau}_s = C_d \rho_a \left| \vec{V}_w \right| \vec{V}_w \tag{3}$$

where ρ_a , C_d , and \vec{V}_w are the air density, wind drag coefficient, and wind velocity at 10 m above the sea surface, respectively. The calculation of the default wind drag coefficient in the FVCOM is based on the formula proposed by Large and Pond (1981):

$$C_d \times 10^3 = \left\{ \begin{array}{ll} 1.2 & \left| \vec{V}_w \right| \leq 11.0 \\ 0.49 + 0.065 \left| \vec{V}_w \right| & 11.0 \leq \left| \vec{V}_w \right| \leq 25.0 \\ 0.49 + 0.065 \times 25 & \left| \vec{V}_w \right| \geq 25.0 \end{array} \right\} \tag{4}$$

The FVCOM’s ability to accurately solve scalar conservation equations and the topological flexibility provided by the unstructured meshes make it perfectly suited for the GBA. The user manual, which is available on the FVCOM website (http://fvcom.smast.umassd.edu/wp-content/uploads/2013/11/MITSG_12-25.pdf), provides a detailed description of the FVCOM.

The high-resolution GBASSP was developed by configuring the updated code of the FVCOM for the GBA, including the wet/dry treatment for the intertidal zones. The computational domain of this model ranges from 110.8°E to 118.5°E and from 19.0°N to 24.0°N. It covers the GBA, the east coast of Guangdong Province, and the coasts of the cities of Yangjiang and Maoming, and it is bounded by an open boundary in the South China Sea (Fig. 3). The model extends from a coarse grid in the open boundary ocean where tides and sea level changes are introduced to an appropriate high resolution (80–100 m) in the Pearl River Delta (PRD) Estuary. The horizontal resolution (measured by the shortest line of a triangle) varies from 0.08 to 0.6 km inside the PRD to 1.0–3.0 km on both sides of the PRD coastal region and to 18.0 km in the area of the South China Sea (SCS) closest to the open boundary. There are a total of 115,642 vertices and 225,336 triangular elements.

The water depth of the model is shown in Fig. 4. 10 uniform sigma layers determine the vertical resolution and are ~0.1 m or less in the intertidal zone and ~2.0 m on the continental shelf. The tidal elevation drives the GBASSP at the open boundary through the Ohio State University TOPEX/Poseidon Global Inverse Solution (OSU TPXO) Tide Models (Egbert

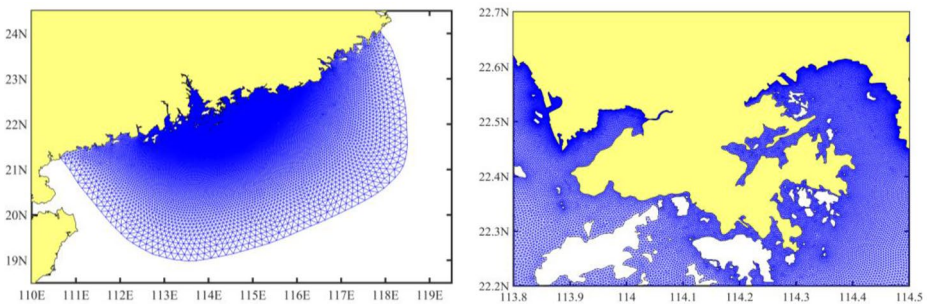


Fig. 3 The grid setup of the Guangdong–Hong Kong–Macao Greater Bay Area storm surge prediction model (GBASSP). It is an unstructured triangular grid, and the resolution gradually transitions from 18 km at the open boundary in the ocean to 0.08–0.6 km in the GBA

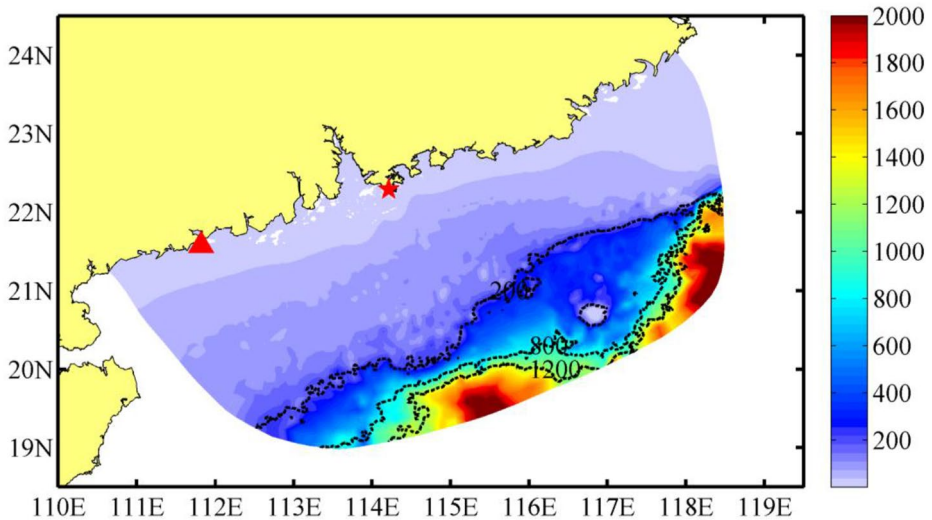


Fig. 4 Bathymetric chart of the Guangdong–Hong Kong–Macao Greater Bay Area storm surge prediction model (GBASSP). The shading denotes the bathymetry; the contours are 200 m, 800 m, and 1200 m

and Erofeeva 2002), which include thirteen major tidal constituents. The external and internal mode time steps are 2.0 and 10.0 s. The wind and air pressure drives of the GBASSP are from the operational GRAPES-3 km model.

2.1.2 Atmospheric model (GRAPES-3 km)

The atmospheric model of the GBASSP is the GRAPES. The numerical prediction system was independently developed by the China Meteorological Administration (CMA). It has fully compressible equations, height-based terrain-following coordinates, and non-hydrostatic equations (details are provided at https://www.cma.gov.cn/en/NewsReleases/MetInstruments/201403/t20140327_241784.html). It performs well regarding both the TC track and TC intensity (Zhang 2018; Zhong et al. 2020; Tan et al. 2022). The latest generation of the GRAPES model includes several improvements, including a new model algorithm, a cloud-based mass flux in the cumulus parameterization, and a new orographic drag parameterization scheme (Zhong and Chen 2015; Chen et al. 2016). GRAPES has been incorporated into three systems in the Guangdong Provincial Key Laboratory of Regional Numerical Weather Prediction. One such system is called GRAPES-MARS, a mesoscale atmospheric regional model system. It is a stand-alone model with a 0.03° horizontal resolution and 56 vertical levels. We used the GRAPES-MARS model (from now on, GRAPES-3 km) as our operational storm surge prediction model's atmospheric model.

2.2 Data

The grid bathymetric data were obtained from the General Bathymetric Chart of the Oceans (GEBCO) database. This global terrain model for oceans and land provides elevation data in

meters on a 15 arc-second interval grid (Mumaw et al. 2023). The data can be downloaded at https://www.gebco.net/data_and_products/gridded_bathymetry_data/.

The lateral boundary conditions are the specified elevations calculated using the harmonic tidal constituents extracted from the OSU TOPEX/Poseidon Global Inverse Solution (TPXO) (Egbert and Erofeeva 2002). It is a current version of a global model of ocean tides, which best fits the Laplace Tidal Equations and along-track averaged data in a least-squares sense. The tides are provided as complex amplitudes of the earth-relative sea-surface elevation for eight primary (M2, S2, N2, K2, K1, O1, P1, and Q1), two long period (Mf and Mm), and three non-linear (M4, MS4, and MN4) harmonic constituents. It can be downloaded at http://g.hyyb.org/archive/Tide/TPXO/TPXO_WEB/global.html.

The observed water level data were obtained from the Intergovernmental Oceanographic Commission (IOC) of the United Nations Educational, Scientific, and Cultural Organization (UNESCO). It can be downloaded at <http://www.ioc-sealevelmonitoring.org/list.php>. The objectives of this service are (i) to provide information about the operational status of global and regional networks of real-time sea level stations and (ii) to provide a display service for quick inspection of the raw data stream from individual stations (Flanders Marine Institute and IOC, 2023). In this study, we used the station of the data for Quarry Bay and Zhapo (Fig. 1) to verify our results because no data are usually available for the other stations around the GBA.

The TC track data were obtained from the CMA best-track data (Lu et al. 2021). Since the most representative typhoons that have affected the GBA in recent years are Typhoon Hato (1723) (Li et al., 2018), Typhoon Mangkhut (1822) (Choy et al., 2020), and Typhoon Higos (2007) (Li et al., 2023), we chose them for the model performance research.

2.3 Methods

To test the GBASSP's ability to physically simulate an entire storm surge event, we examined several storm surges induced by different typhoons in recent years.

According to technical directives for assessment and zoning of marine disaster (Ministry of Natural Resources of the People's Republic of China, 2019), we divided the storm surges into five levels: normal (V, 0.5–1 m storm surges), moderate (IV, 1–1.5 m), fairly strong (III, 1.5–2 m), strong (II, 2–2.5 m), and extra strong (I, >2.5 m).

We studied the results for different start times to further evaluate the model's performance. In this study, we focused on the early warning capability of the GBASSP, so the research period was mainly concentrated at least 24 h before the typhoon's landfall. Fct24, Fct36, Fct48, Fct60, and Fct72 denote the results for start times of 24, 36, 48, 60, and 72 h before typhoon landfall time, respectively. To verify the system's ability, we calculated the maximum error (ME), absolute error (AE), relative error (RE), and root mean square error (RMSE) between the forecasted and observed water levels using Eqs. (5)–(8):

$$ME = \max(F_i) - \max(O_i), \quad (5)$$

$$AE = \text{abs}(F_i - O_i), \quad (6)$$

$$RE = \frac{AE}{O_i} \times 100\%, \quad (7)$$

$$RMSE = \sqrt{\frac{1}{n} \sum_{i=1}^n (F_i - O_i)^2}, \tag{8}$$

where n is the number of forecasted and observed values, O_i is the observed water level, and F_i is the forecasted water level.

3 Performance of GBASSP

3.1 Overview of typhoons Mangkhut, Hato, and Higos

We conducted independent case studies for typhoons Hato (1713), Mangkhut (1822), and Higos (2007). These typhoons were chosen because they are the most representative typhoons that affected the GBA in recent years.

Among the selected typhoons (Fig. 5), Super Typhoon Mangkhut was the strongest to approach and make landfall in the PRD in recent years; thus, we use it as an example. Typhoon Mangkhut formed over the western North Pacific east of Guam on September 7, 2018. It reached its peak intensity before landfall over Luzon, with a maximum sustained wind speed of 65 m s^{-1} near the center. Mangkhut weakened after crossing the northern part of Luzon and continued to travel northwestward across the north part of the SCS toward the GBA. Mangkhut weakened to a severe typhoon and finally made landfall in Jiangmen in the GBA at 09:00 UTC on September 16, 2018. It then moved into the western part of Guang-

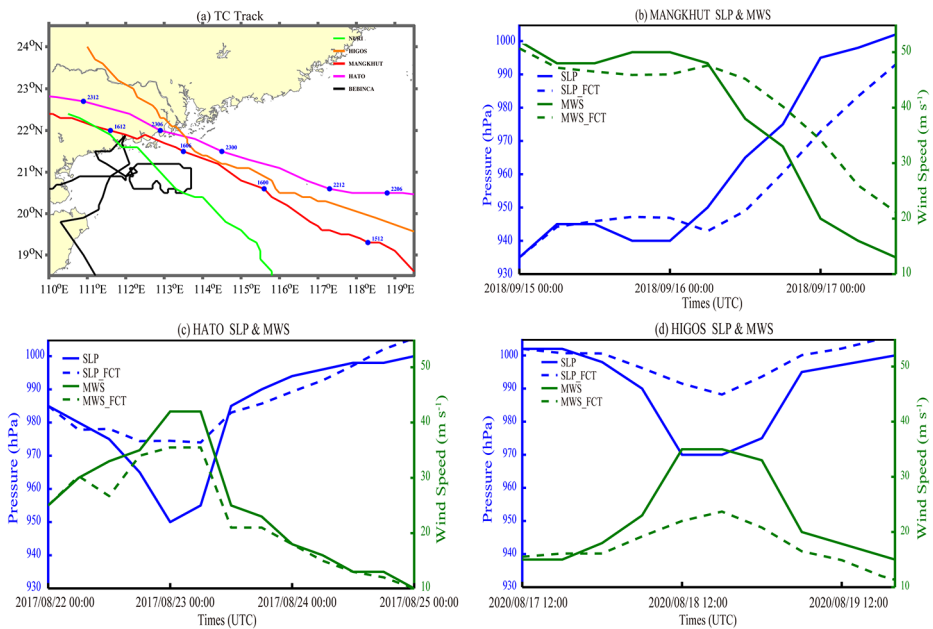


Fig. 5 Comparison of the tracks (a) and intensities (b)–(d) of the three TCs. The interval between two adjacent points on the same line is 6 h. FCT indicates the track and intensity forecast from GRAPES-3 km, while SLP and MWS in (b)–(d) represent the sea level pressure and maximum wind speed around the TC center, respectively

dong and degenerated into a low-pressure system over Guangxi Province the next day. It forced Hong Kong to issue the highest tropical cyclone warning signal, the No. 10 Hurricane Signal. Mangkhut caused the most severe and widespread destruction in recent decades. The maximum sea level (the sum of the astronomical tide and storm surge) in Quarry Bay rose to 3.88 m, which was only 0.08 m lower than Wanda's record high of 3.96 m induced in 1962. As a result, many coastal areas in the GBA suffered severe inundation.

Super Typhoon Hato was the strongest typhoon that landed in China in 2017, and it formed a tropical depression over the eastern part of Luzon at 18:00 UTC on August 19, 2017. The next day, it developed into the 13th named storm in 2017 and moved west-northwest. On August 22, it passed over the northern portion of the SCS and reached typhoon intensity. It intensified and became a strong typhoon with a maximum wind speed of 52 m s^{-1} and a central pressure of 935 hPa at 03:00 UTC on August 23. Typhoon Hato went through a 27-hour intensification period, with a deepening rate of 27 m s^{-1} (50 hPa) from 00:00 UTC on August 22 to 03:00 UTC on August 23. Approximately 2 h later, at 04:50 UTC on August 23, it made landfall in Zhuhai, Guangdong Province, with a maximum wind speed of 45 m s^{-1} and a central pressure of 950 hPa. It weakened over land and dissipated on August 24 in Yunnan Province, China. Hato caused violent winds and a severe storm surge on the coast of the Pearl River Estuary, especially in Macao and Zhuhai. Extensive areas of Macao, including some underground car parks, suffered from severe flooding and damages, resulting in at least ten deaths and more than 240 injuries (Li et al. 2018).

Typhoon Higos was the weakest typhoon among the three cases, but it also reached typhoon level (with a maximum wind speed of 35 m s^{-1}). It formed east of the Philippines on August 16, 2020, and moved northwest. It continued to intensify and was named in the northern part of the SCS on August 18. At 22:00 UTC on August 18, it made landfall in Zhuhai, Guangdong Province, and nearly reached its peak intensity (with an observed wind speed of 35 m s^{-1}). After it made landfall, Higos continued to move northwest, and it gradually weakened to a tropical depression at 12:00 UTC on August 19 in Guangxi Province. A fast movement speed and rapid offshore intensification characterized it. Typhoon Higos underwent a very intense and short intensification period, with a deepening rate of 5 hPa/h from 08:00 UTC to 12:00 UTC on August 18. The storm surge by Higos resulted in an estimated \$49 million RMB in direct economic damage, not including indirect losses from suspending economic activity such as port closures and flight cancellations.

The forecast error for Typhoon Mangkhut was minimal regarding track and intensity, with the difference in maximum wind speed (MWS) at landfall being only 5 m s^{-1} . Although the model predicted that typhoons Hato and Higos would increase in intensity near the coast, the magnitude of the predicted increase was significantly smaller than the observation. However, compared to typhoon Hato, the error in the predicted track of typhoon Higos was smaller before it made landfall. Thus, regarding storm surge forecasting, Typhoon Hato exhibited more evident deviation between the predicted and observed results (refer to Sect. 3.2 for detailed information).

3.2 Case verification

We examined the storm surges induced by the above three typhoons to test the GBASSP's ability to physically simulate an entire storm surge event.

3.2.1 Typhoon Mangkhut

During Super Typhoon Mangkhut, the storm surge along the coast of the GBA was prominent (Fig. 6b). The significant storm surge area was located along the coast, from Huangmao Sea to Daya Bay, and the maximum water increase occurred in the PRE, with a maximum value of greater than 3 m at 13:00:00 on 2018-09-16. The storm surge was more significant in the eastern part of the PRE than in the part of the west. At this time, the typhoon made landfall, and the center was located ~60 km from the coastline (Fig. 5). The strong south/southeast wind on the southeast side of the typhoon caused high winds from the Huangmao Sea to the PRE (Fig. 6a), which induced a significant storm surge in this area (Fig. 6b). The most significant storm surge within the PRE was related to the trumpet-shaped topography, i.e., the land was closer and the channel was narrower.

We also compared the water level series at the different stations. It can be seen that the predicted water levels are in good agreement with the observations for both stations (Fig. 7). First, the periodic oscillation of the water level is well simulated, except that there is a slight difference in the extreme values (peaks and troughs) between the observations (Obs) and the forecasted values (Fct). Second, the maximum storm surge, the critical variable we are most interested in, is also well reproduced. The discrepancy with the observations is around 5 cm (the maximum difference during the grey-shaded period in Fig. 7). The results are better closer to the landfall time (the red line (Fct24) is closer to the observations than both the green (Fct72) and blue (Fct48) lines). Third, the results for Quarry Bay are better than those for Zhapo station. For the Quarry Bay station, the model can predict the storm surge about three days in advance, while for Zhapo station, it can predict the storm surge about two days in advance. It should be noted that for Zhapo station, the results are not good from 04:00:00 on 2018-09-16 to 12:00:00 on 2018-09-16.

To verify the warning capability of the GBASSP model, we produced Fig. 8. As can be seen from Fig. 8, the model forecasted a strong storm surge in the GBA since 00:00 UTC on September 14, 2018, which was at least 2 days in advance of when Typhoon Mangkhut made landfall (Mangkhut made landfall at 09:00 UTC on September 16, 2018). The most severe storm surges occurred in the PRE and on the east bank of the estuary, reaching more than 2.5 m. The results are consistent with the data from the Quarry Bay observation station.

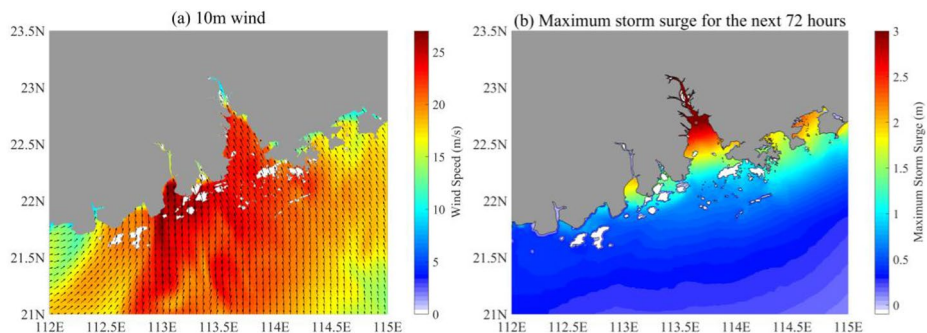


Fig. 6 The distributions of (a) the wind speed at 10 m and (b) the storm surge when the maximum storm surge occurred (13:00:00 on 2018-09-16) during Typhoon Mangkhut from the results of Fct24. Fct24 denotes the results from the start time of the model, which is at least 24 h before Mangkhut made landfall. The time 2018-09-16 13:00:00 is when the increase in the water level in the model domain reached the maximum value during Typhoon Mangkhut

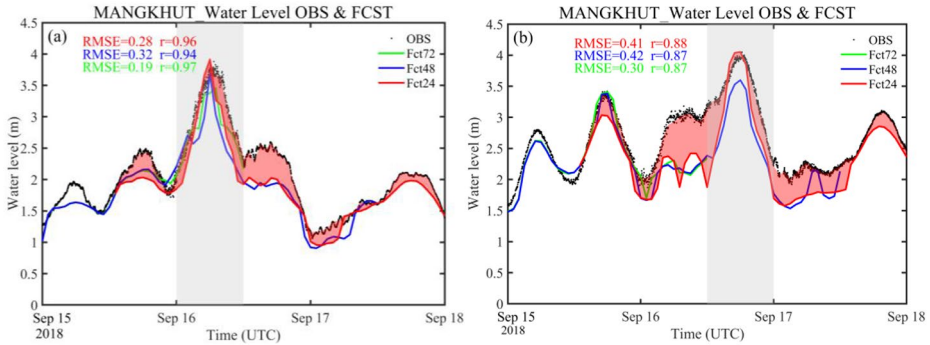


Fig. 7 Series of forecasted and observed water levels during Typhoon Mangkhut at (a) Quarry Bay station and (b) Zhapo station. OBS denotes the observations. Fct72 indicates that the model’s forecast results are from the start time of the model, which is at least 72 h in advance of Typhoon Mangkhut’s landfall time, and Fct48 and Fct24 indicate 48 and 24 h in advance, respectively. The gray shading denotes the period (10 h before and after the maximum storm surge occurred at each site). The red shading represents the difference between the observations and Fct24

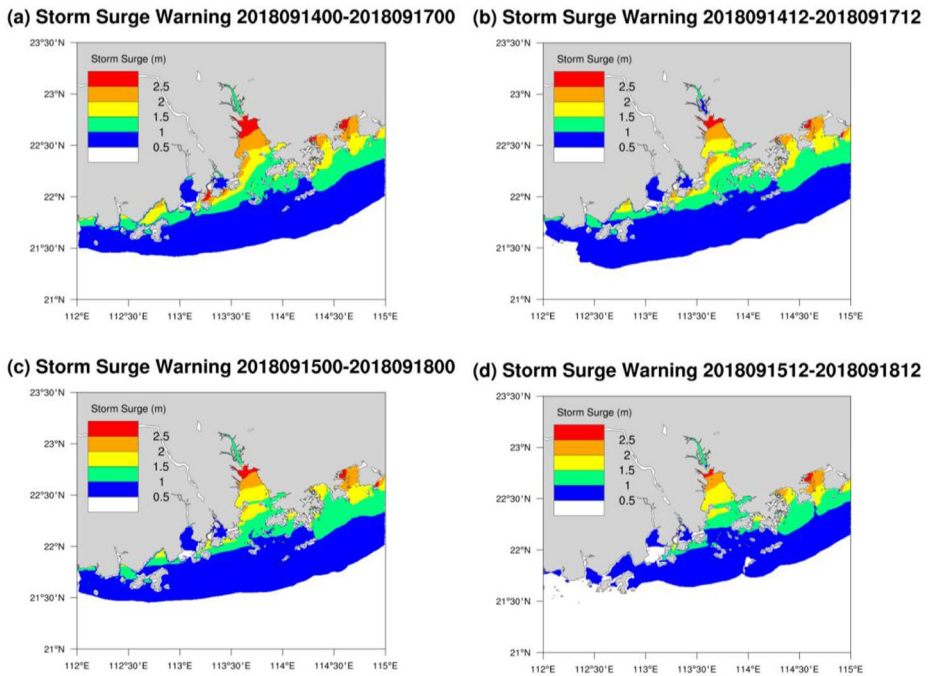


Fig. 8 Storm surge warning for the next 72 h for Typhoon Mangkhut obtained from the GBASSP model. The number in the title is a date in the YYYYMMDDHH format, where YYYY is the year, MM is the month, DD is the day, and HH is the hour. For example, 2,018,091,400 denotes 00:00 UTC on September 14, 2018

3.2.2 Typhoon Hato

For Typhoon Hato, the predicted storm surge was not as strong as that caused by Mangkhut, but it was still significant along the coast of the GBA (Fig. 9b). The most significant area of the storm surge was located in the PRE and Daya Bay, with a maximum value of greater than 2 m at 04:00:00 on 2017-08-23. The storm surge on the east side of the PRE was also more significant than that on the west side of the PRE. The typhoon had not yet made landfall, and the center was located ~ 40 km from the coastline in the model (Fig. 9a). The strong southeast/north wind on the northeast/northwest side of the typhoon caused high winds from Daya Bay to the PRE (Fig. 9a), which induced a significant storm surge in this area (Fig. 9b). It should be noted that the forecast obtained from the GBASSP's atmospheric model (GRAPES-3 km) was not good at this time. According to the observations, Hato went through a 27-hour intensification period when it was 100 km offshore before landfall, with a deepening rate of 27 m s^{-1} (50 hPa) from 00:00 UTC 22 to 03:00 UTC on August 23, and the maximum wind speed reached 52 m s^{-1} , while the maximum wind speed forecasted by the model was 40 m s^{-1} , which led to the forecasted storm surge being weaker than the observations.

As was previously mentioned, the forecast of the intensity of Typhoon Hato in the GRAPES-3 km is not as good as that for Mangkhut, and the predicted water levels have a more significant error than that for Mangkhut (Fig. 10). However, the periodic oscillation of the water level is also well simulated (correlation coefficients of greater than 0.96), and the water level forecast at Zhapo station is consistent with the observations. The maximum error of the storm surge at Zhapo station is almost zero, while the anomaly of Quarry Bay is approximately -1 m. Similarly, as the forecast start time increased, the error became smaller (the red line (Fct24) is closer to the observations than both the green (Fct72) and blue (Fct48) lines). Unfortunately, the results for Quarry Bay are only slightly improved due to the poor forecasting of the wind field of GRAPES-3 km. Although, in this case, the anomaly of the maximum storm surge in Quarry Bay is large, the model can forecast the storm surge three days in advance at both stations.

The GRAPES-3 km model exhibited a weak performance in forecasting the rapid intensification of Typhoon Hato, with the predicted surge area at 12:00 UTC on August 20, 2017, being very small, as shown in Fig. 11(a). The resolution around the GBA was very high,

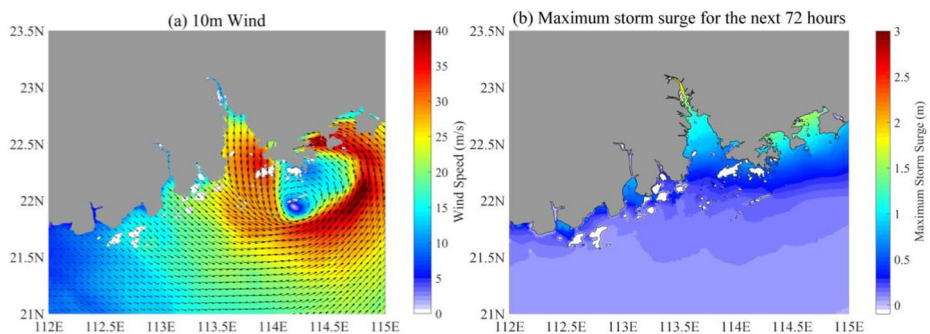


Fig. 9 Same as in Fig. 6, but for Typhoon Hato. The distributions of (a) the wind speed at 10 m and (b) the storm surge. The maximum storm surge occurred at 04:00:00 on 2017-08-23 during Typhoon Hato based on the results of Fct24

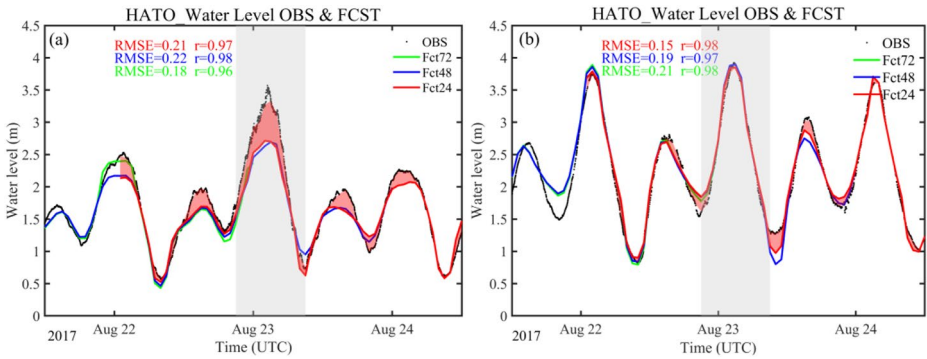
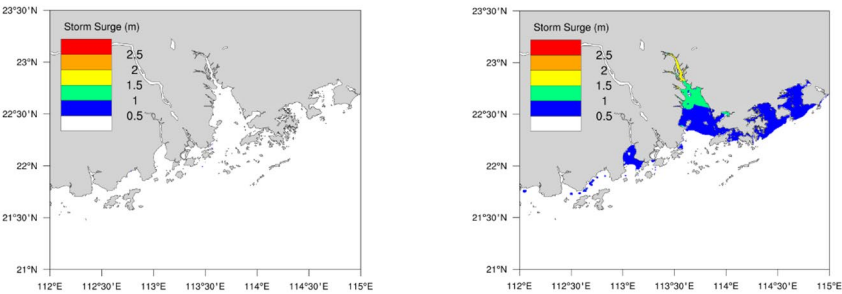


Fig. 10 Same as in Fig. 7, but for Typhoon Hato. Series of the forecasted and observed water levels during Typhoon Hato. (a) Quarry Bay station, and (b) Zhapo station

(a) Storm Surge Warning 2017082012-2017082312 (b) Storm Surge Warning 2017082100-2017082400



(c) Storm Surge Warning 2017082112-2017082412 (d) Storm Surge Warning 2017082200-2017082500

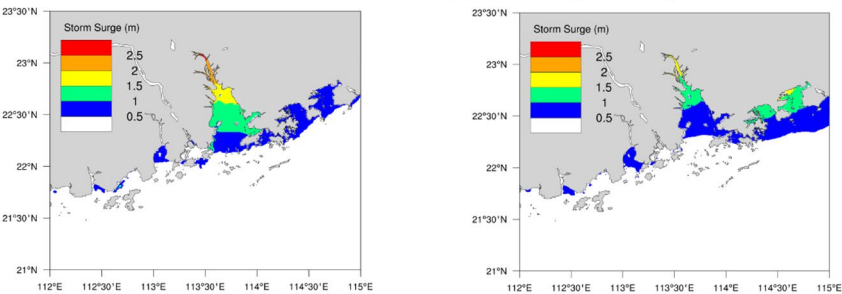


Fig. 11 Same as in Fig. 8, but for Typhoon Hato. The number in the title is a date in the YYYYMMDDHH format, where YYYY is the year, MM is the month, DD is the day, and HH is the hour. For example, the number 2,017,082,012 denotes 12:00 UTC on August 20, 2017

and by enlarging Fig. 11(a), it becomes apparent that there were several blue dots outside the southwest side of the Pearl River Delta (at about 113.5°E and 22°N), indicating that the surge in this region was about 0.5–1 m. In summary, the model forecasted strong storm surges in the PRE and on the east bank of the estuary at least 2 days before landfall (Hato made landfall at 04:50 UTC on August 23, 2017). The most severe storm surge (>2 m) occurred in the PRE and on the east bank of the estuary. Due to the weaker forecast wind,

the storm surge was weaker in the model compared to the observations (e.g., the observed storm surge in Quarry Bay was 1.18 m and the model forecast was 0.78 m).

3.2.3 Typhoon Higos

During Typhoon Higos, the storm surge was only evident around the landing area (Zhuhai) (Fig. 12b). A significant storm surge occurred along the coasts of Guanghai Bay and Zhuhai, with a maximum value of ~ 3 m. The typhoon center moved northwest to Yangjiang after landing in Zhuhai (Fig. 5), so the storm surge was more significant in the PRE's western part than in the PRE's eastern part. The strong south wind on the east side of the typhoon caused high winds along Zhenhai Bay and Guanghai Bay, which induced a significant storm surge in this region (Fig. 12a). The storm surge within the PRE was much smaller due to the lower wind speed in this area.

It is clear that in general, the water level forecast obtained from the GBASSP is accurate for Higos, and both the amplitude and period are consistent with the observations (Fig. 13). In addition, the forecast for Typhoon Higos is better than that for Super Typhoon Mangkhut. Moreover, compared with the error at Zhapo Station, the error at the Quarry Bay Station is larger, since Quarry Bay is located between several islands in Hongkong. The error of the water depth data in the model is greater than that in Zhapo (because the water depth is interpolated from the GEBCO, the grid in Quarry Bay has a higher resolution), so the forecast results are slightly worse than those for Zhapo. In this case, the model can forecast the storm surge three days in advance at both stations.

For the weaker Typhoon Higos (Fig. 14), the model can forecast the storm surge around the landfall area approximately 2 days in advance (Higos made landfall at 22:00 UTC on August 18, 2020). The most server storm surge occurred on the western coast of the PRE, which is located in the typhoon landfall region. As can be seen from Figs. 8 and 11 and, 14, the model basically provides storm surge early warning for the public 2 days in advance and as times goes on, the warning results become increasingly more accurate.

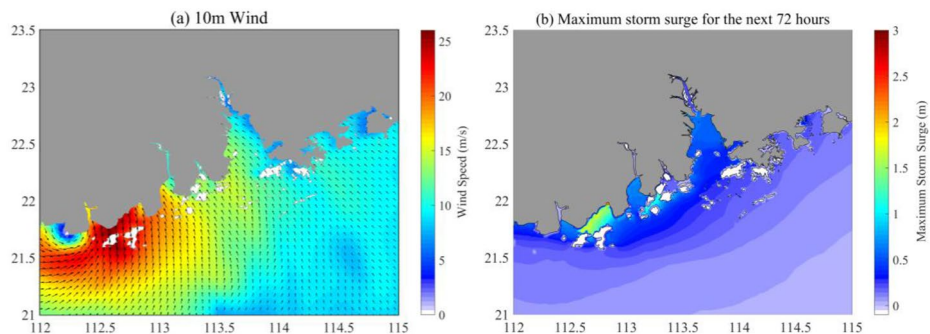


Fig. 12 Same as in Fig. 6, but for Typhoon Higos. The distributions of (a) the wind speed at 10 m and (b) the increase in the water level when the maximum storm surge occurred (00:00:00 on 2020-08-19) during Typhoon Higos from results for Fct24

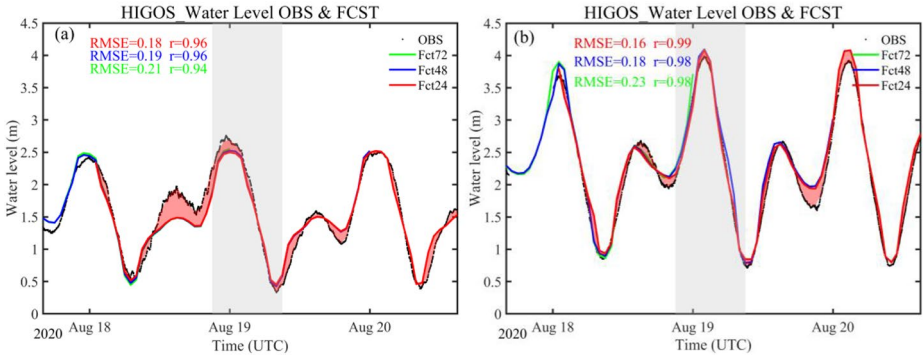


Fig. 13 Same as in Fig. 7, but for Typhoon Higos. Series of forecast and observed water levels during Typhoon Higos. **(a)** Quarry Bay station, and **(b)** Zhapo station

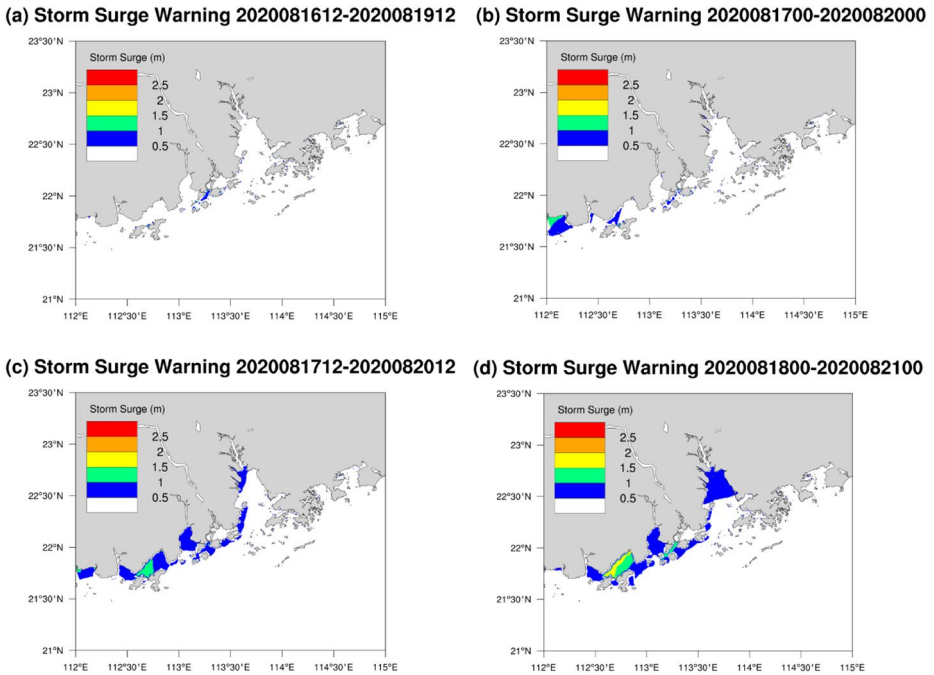


Fig. 14 Same as in Fig. 8, but for Typhoon Higos. The number in the title is a date in the YYYY-MMDDHH format, where YYYY is the year, MM is the month, DD is the date, and HH is the hour. For example, the number 2,020,081,612 denotes 12:00 UTC on August 16, 2020

4 Evaluation of key indicators

Based on previous studies (Needham et al. 2015; Feng et al. 2016; Chu et al. 2019), we chose the maximum storm surge error, error of the occurrence time of the maximum storm surge, RMSE, absolute error, and relative error as key indicators to evaluate the performance of the model.

4.1 Maximum storm surge verification

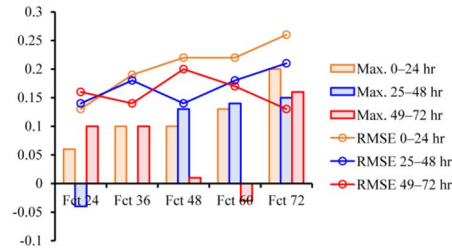
To assess the accuracy of the model in predicting storm surges, we analyzed the maximum storm surges caused by the selected typhoons. We compared the observed and forecasted water levels, as well as their corresponding occurrence times at both the Quarry Bay station and Zhapo station (Table 2). First, we considered the maximum storm surge. Except for at Quarry Bay station, during Typhoon Hato, the forecasted values are consistent with the observed levels at both Quarry Bay station and Zhapo station. The difference between the forecasted and observed values ranged from 0.02 to -1.17 m, with a particularly low deviation of less than 25 cm for the Fct24 results, except for Typhoon Hato. As was previously mentioned, because the GRAPES-3 km is not accurate enough in predicting the rapid intensification of Hato, the maximum error (-117 cm) occurs for the Fct72 results for Strong Typhoon Hato. Although the model error is large at this time, it is significantly lower for other forecast start times. On average, the model error gradually decreases as the forecast time progresses. It decreases from 42.5 cm for Fct72 to 19.7 cm for Fct24. This trend may be due to the improved accuracy of the prediction results of the driving field as the landing time progresses. Additionally, it should be noted that the time resolution of the model is 1 h, and the error of the occurrence time of the maximum storm surge between the observations and model results is within 1 h (except for two Fct72 results from a total of 18 results). Therefore, the occurrence time of the maximum storm surge obtained from the model is close to the observed time.

Table 2 Comparison of the maximum water level for the observations (Obs) and GBASSP forecast results for the different typhoons

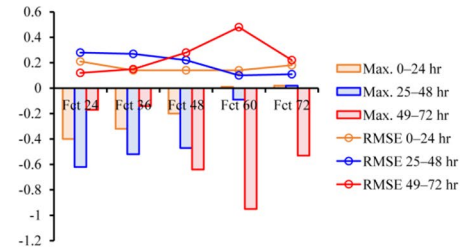
Typhoon	Obs (m) & occurrence Time	Fct24*/anomaly (m) & occurrence Time	Fct48*/ anomaly (m) & occurrence Time	Fct72*/ anomaly (m) & occurrence Time	Station
Hato	3.57 2017-08-23 02:27:00	2.71/ -0.86 2017-08-23 02:00:00	2.69/ -0.88 2017-08-23 03:00:00	2.40/ -1.17 2017-08-23 02:00:00	Quarry Bay
	3.94 2017-08-23 02:44:00	3.85/ -0.09 2017-08-23 03:00:00	3.90/ -0.04 2017-08-23 03:00:00	3.89/ -0.05 2017-08-23 02:00:00	
	3.88 2018-09-16 06:42:00	3.92/0.04 2018-09-16 06:00:00	3.68/ -0.2 2018-09-16 06:00:00	3.46/ -0.42 2018-09-16 07:00:00	Quarry Bay
	4.05 2018-09-16 18:18:00	4.00/ -0.05 2018-09-16 18:00:00	3.60/ -0.45 2018-09-16 18:00:00	3.44/ -0.61 2018-09-13 16:00:00	
Higos	2.76 2020-08-18 23:22:00	2.52/ -0.24 2020-08-18 23:00:00	2.53/ -0.23 2020-08-19 00:00:00	2.55/ -0.21 2020-08-19 00:00:00	Quarry Bay
	3.99 2020-08-19 01:55:00	4.01/0.02 2020-08-19 02:00:00	4.10/0.11 2020-08-19 02:00:00	3.90/ -0.09 2020-08-18 01:00:00	
	Mean absolute error	--	--/0.197	--/0.282	--/0.425

* Fct24, Fct48, and Fct72 denote the results when the start-time of the GBASSP is at least 24, 48, and 72 h before the typhoon landfall time, respectively

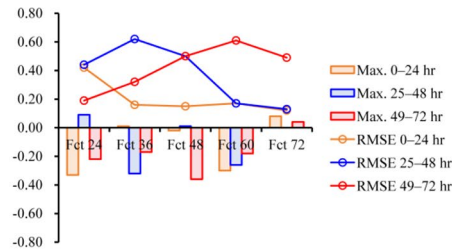
(a) Hato, Zhapo



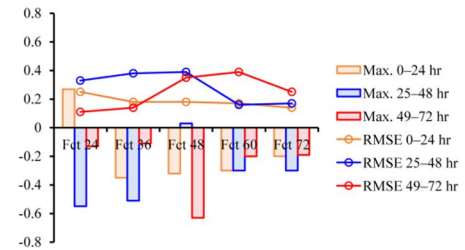
(b) Hato, Quarry Bay



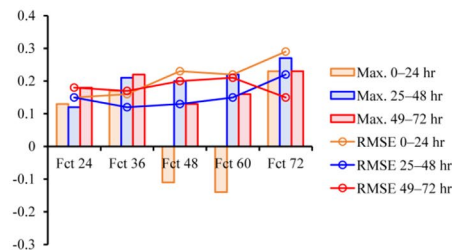
(c) Mangkhut, Zhapo



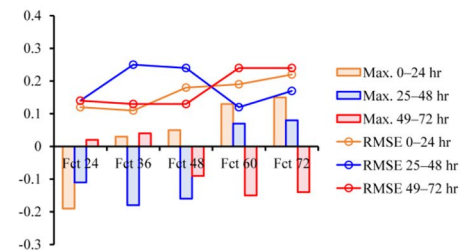
(d) Mangkhut, Quarry Bay



(e) Higos, Zhapo



(f) Higos, Quarry Bay



(g) Mean

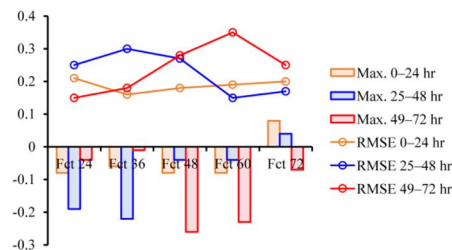


Fig. 15 Root mean square error (RMSE) and maximum error (Max) of the GBASSP results at Quarry Bay station and Zhapo station during typhoons Hato (a–b), Mangkhut (c–d), Higos (e–f), and the mean values of the three typhoons of two stations (g). Fct24, Fct36, Fct48, Fct60, and Fct72 denote the results of the GBASSP for start times of at least 24, 36, 48, 60, and 72 h before typhoon landfall time, respectively

4.2 RMSE and ME verification

In addition, to evaluate the model performance in detail, the root mean square error and the maximum storm surge error of the GBASSP were calculated for the two sites during the selected TCs (Fig. 15). On average, the RMSE of the GBASSP was relatively stable, ranging from 15 to 35 cm (Fig. 15g). The error of the maximum water level, the most critical variable we are interested in, has a good performance, and all of the errors are less than 27 cm. In particular, for 12 of the 15 results, the error is less than 10 cm for any forecast start time (i.e., 0–24 h, 25–48 h, and 49–72 h). With the advancement of the start time of the model, the RMSE and ME do not exhibit significant decreasing trends; that is, sometimes they decrease (e.g., the RMSE for 0–24 h decreases from 0.18 m for Fct48 to 0.16 m for Fct36) and sometimes they increase (e.g., the RMSE for 0–24 h increases from 0.16 m for Fct36 to 0.21 m for Fct24). However, as the effective forecast time increases, the RMSE gradually increases, i.e., the forecast for 0–24 h is better than that for 49–72 h. In detail, the forecast for Quarry Bay station seems to be poorer than that for Zhapo station. On average, the RMSE for Quarry Bay varies between 10 and 48 cm, with almost the same average value as that for Zhapo station (~20 cm). The ME is slightly higher than that for Zhapo station, especially during Typhoon Mangkhut. The RMSE and ME of the forecasts for 0–24 h and 25–48 h are only slightly different, indicating that the prediction skills of the model are similar for these two forecast periods.

4.3 Comparison with other models

Third, we also compared the GBASSP with other prediction models (Table 3). It can be seen that the average RE and RMSE of the GBASSP are 5.9% and 21 cm, respectively, which are the smallest of all of the models. In addition, the average AE is between those of the other models. It should be noted that the resolutions of the GBASSP, Chu's, Han's, Zhang's, and Xiong's models are 80–100 m, 500 m, 100 m, 5–10 m, and 5 km, respectively. Our model has more minor errors than the model including the GBA (Xiong et al. 2022). The storm surge results are sensitive to the grid resolution (Sasaki and Iizuka 2007; Kohno et al. 2018); thus, the error of Xiong's model is the largest. Hurricane winds are the primary driver of storm surges. The wind fields of Han's model and Zhang's model are extracted from the Holland model (Holland 1980), while the wind fields of the GBASSP and Chu's model are extracted from more actual forecast wind fields, such as the GRAPES and the fifth generation European Centre for Medium-Range Weather Forecasts (ECMWF) atmospheric reanalysis of the global climate (ERA5). Therefore, the results of the GBASSP and Chu's model are better than those of the other two. Due to its higher resolution, the GBASSP has better forecasting skills than Chu's model.

Table 3 Comparison of forecast maximum storm surge for the next 24 h

	GBASSP	Chu's model (2019)	Han's model (2019)	Zhang's model (2021)	Xiong's model (2022)
RMSE (cm)	21	33	--	--	--
Average absolute error (cm)	19.7	--	18.1	18.0	35.5
Average relative error (%)	5.9	7.0	12.9	7.5	18.9

5 Conclusions and discussion

The GBA is the largest urban agglomeration in the world. Still, it is located in a low-lying, flood-prone coastal area exposed to sea level rise and extreme water levels generated by typhoon-induced storm surges. In this study, we developed a coupling model to forecast the typhoon-induced storm surges in the GBA. First, based on an ocean model (FVCOM) and atmospheric model (GRAPES-3 km), we constructed a real-time storm surge prediction system for the GBA, namely, the GBASSP. Second, we analyzed the model's performance for typhoons Mangkhut, Hato, and Higos. Finally, we evaluated the early warning capability of the GBASSP. The main conclusions are as follows.

(1) The high-resolution GBASSP was developed by configuring the updated code of an unstructured grid model (FVCOM) for the GBA and coupling the wind and pressure fields of the GRAPES-3 km. It is a new attempt to establish a GBASSP with a maximum horizontal resolution of 80 m for storm surge warnings in the GBA.

(2) The GBASSP can provide early warning and forecasting, and it can give storm surge early warning at least 2 days before typhoon landfall. For Typhoon Mangkhut, it forecasts a maximum storm surge of ~4 m, with an error of less than 5 cm at both Zhapo station and Quarry Bay station. For Typhoon Higos, the error is ~20 cm at Quarry Bay station and 2 cm at Zhapo station. For Typhoon Hato, the error of the maximum storm surge at Quarry Bay station is ~80 cm (results of Fct24), while the error at Zhapo station is less than 10 cm. This increase in error is mainly due to the weak forecast wind field of the GRAPES.

(3) The key performance indicators of the model indicate that it performs well. The RMSE of the GBASSP is relatively stable on average, ranging from 15 to 35 cm, with an average RMSE of 21 cm. The mean absolute error of the maximum storm surge is 19.7 cm in the next 24 h, and it gradually increases as the effective forecast time increases. In addition, the maximum storm surge occurrence time difference between the observations and the results of the GBASSP is mostly within 1 h. It should be noted that the prediction skills of the model are similar for the 0–24 h and 25–48 h forecast periods at the two stations. Our model has the best forecasting skill compared to other storm surge prediction models. The relative error and root mean square error of the GBASSP are 5.9% and 21 cm, respectively, the smallest of all of the models, while the average absolute error is between those of the other models.

The GBASSP has several advantages. First, it can more accurately simulate tidal elevations, residual currents, and water levels than other models by using an unstructured triangular mesh to better represent the complex distribution of sea and land terrain features in the GBA (Chen et al. 2003; Passeri et al. 2015). Second, the time from the initiation of the system to the end of the model's runtime is ~100 min. This is fast enough to meet operational requirements, and in the near future, the runtime of the GBASSP is expected to be reduced to half of what it currently is through more computational cores. Third, compared to other forecast systems (Table 3), the GBASSP performs well and has the best forecasting ability. The relative and root mean square errors of the GBASSP are 5.9% and 21 cm, respectively, the smallest of all the comparative models used in this study.

We found that the model still has some areas for improvement. First, the GRAPES are not good under the rapid intensification of Typhoon Hato, and thus, the error for Typhoon Hato is more significant than those for the other cases. Wind stress is the dominant factor that affects storm surges (Akbar et al., 2015; Arns et al. 2017; Shen et al. 2019; De Domini-

cis et al. 2020). To improve this issue, many studies have reported that assimilating observational data can improve typhoon track and intensity forecasting (Liu and Li 2010; Weng and Zhang 2016; Velden et al. 2017; Liu et al. 2018). Therefore, further GRAPES can be improved by assimilating the latest observation data, such as FengYun –4 satellite data, to improve the model. Second, due to the imprecise topography and land use/land cover, the warning along the coast of Guanghai Bay is not continuous for Typhoon Higos (Fig. 14c, d). This result demonstrates the significant influence of changes in the landscape, consistent with previous research results (Bilskie et al. 2014; Passeri et al. 2015). Hence, the following improvement step, i.e., including high resolution topographic data such as chart data, will be addressed and tested in a future study. Third, in this study, the bottom friction and wind drag coefficient were acquiescent (see formulas (2) and (4) in Sect. 2.1.1); however, storm surges are sensitive to them (Bunya et al. 2010; Peng and Li 2015; Akbar et al. 2017). In future work, we will test many different parameters to determine the most appropriate combination of parameters for forecasting storm surges in the GBA. Finally, more observational comparison is needed to better demonstrate the model's prediction performance.

Acknowledgements The authors thank the Marine Meteorological Science Experiment Base at Bohe, Maoming, and Guangdong Provincial Marine Meteorology Science Data Center. We thank Professor Zhigang Lai of Sun Yat-sen University for his valuable advice and support on the establishment of the model.

Author contributions MZ: Formal analysis; Methodology and software; Writing—original draft. CL: Data Curation; Supervision; Resources. GD: Data Curation; Atmospheric model. HH: Conceptualization; Supervision; Writing—review and editing. QS: Supervision; Resources. ML: Data Curation; Atmospheric model.

Funding This study was jointly supported by the National Key R&D Program of China (Grant No. 2023YFC3008001), the Guangdong Provincial Marine Meteorology Science Data Center (Grant No. 2024B1212070014), the science and technology research project of the Guangdong Meteorological Bureau (Grant No. GRMC2022Q02), the China Meteorological Administration Innovation Development project (Grant No. CXFZ2023P040), and the Innovation team of severe weather mechanism and forecasting technology in the South China Sea of the Guangdong Provincial Meteorological Bureau (Grant No. GRMCTD202201).

Data availability The data supporting this study's findings are available upon request from the corresponding authors.

Declarations

Conflict of interest The authors declare that the research was conducted without any commercial or financial relationships that could potentially create a conflict of interest.

References

- Akbar MK, Kanjanda S, Musinguzi A (2017) Effect of bottom friction, wind drag coefficient, and meteorological forcing in hindcast of hurricane Rita storm surge using SWAN+ADCIRC model. *J Mar Sci Eng* 5(3):38. <https://doi.org/10.3390/jmse5030038>
- Androsov A, Fofonova V, Kuznetsov I, Danilov S, Rakowsky N, Harig S et al (2019) FESOM-C v.2: Coastal dynamics on hybrid unstructured meshes. *Geosci Model Dev* 12(3):1009–1028. <https://doi.org/10.5194/gmd-12-1009-2019>
- Arns A, Dangendorf S, Jensen J, Talke S, Bender J, Pattiaratchi C (2017) Sea-level rise induced amplification of coastal protection design heights. *Sci Rep* 7:40171
- Banks JE (1974) A mathematical model of a river-shallow sea system used to investigate tide, surge and their interaction in the Thames-southern North Sea region. *Phil Trans R Soc Lond A275:567–609*

- Bilskie MV, Hagen SC, Medeiros SC, Passeri DL (2014) Dynamics of sea level rise and coastal flooding on a changing landscape. *Geophys Res Lett* 41:927–934. <https://doi.org/10.1002/2013GL058759>
- Bloemendaal N, Muis S, Haarsma RJ et al (2019) Global modeling of tropical cyclone storm surges using high-resolution forecasts. *Clim Dyn* 52:5031–5044. <https://doi.org/10.1007/s00382-018-4430-x>
- Bulletin of China Marine Disaster (2020–2022) Available online at: <https://www.mnr.gov.cn/sj/sjfw/hy/gbgb/zghyghgb/> (accessed June 2, 2021)
- Bunya S, Dietrich JC, Westerink JJ et al (2010) A high-resolution coupled riverine flow, tide, wind, wind wave, and storm surge model for southern Louisiana and Mississippi. Part I: model development and validation. *Mon Wea Rev* 138(2):345–377. <https://doi.org/10.1175/2009MWR2906.1>
- Burchard H (2002) Applied Turbulence modeling in Marine Waters. Lecture Notes in Earth Sci., vol 100. pp., Springer, New York, p 215
- Chen C, Liu H, Beardsley RC (2003) An unstructured grid, finite-volume, three-dimensional, primitive equations ocean model: application to coastal ocean and estuaries. *J Atmos Ocean Technol* 20(1):159–186
- Chen ZT, Dai GF, Zhong SX et al (2016) Technical features and prediction performance of typhoon model for the South China Sea. *J Trop Meteorol* 32(6):831–840. <https://doi.org/10.16032/j.issn.1004-4965.2016.06.005>(in Chinese)
- Choy C-W, Wu M-C, Lee T-C (2020) Assessment of the damages and direct economic loss in Hong Kong due to Super Typhoon Mangkhut in 2018. *Trop Cyclone Res Rev* 9:193–205. <https://doi.org/10.1016/j.tcr.2020.11.001>
- Chu DD, Zhang JC, Wu YS, Jiao XH, Qian SH (2019) Sensitivities of modelling storm surge to bottom friction, wind drag coefficient, and meteorological product in the East China Sea. *Estuarine, Coastal and Shelf Science*, 231, 106460. <https://doi.org/10.1016/j.ecss.2019.106460>
- Cochran J, Kirk HJ, Bokuniewicz, Yager PL (2019) *Encyclopedia of Ocean Sciences (Third Edition)* Editors, Elsevier Ltd
- De Dominicis M, Wolf J, Jevrejeva S, Zheng P, Hu Z (2020) Future interactions between sea level rise, tides, and storm surges in the world's largest urban area. *Geophys Res Lett* 47:e2020GL087002. <https://doi.org/10.1029/2020GL087002>
- Deltares Delft3D-FLOW (2014) Simulation of multi-Dimensional Hydrodynamic Flows and Transport phenomena, including sediments - User Manual
- Egbert GD, Erofeeva SY (2002) Efficient inverse modeling of Barotropic Ocean Tides. *J Atmos Ocean Technol* 19:183–204. [Available online at https://journals.ametsoc.org/view/journals/atot/19/2/1520-0426_2002_019_0183_eimobo_2_0_co_2.xml]
- Emanuel KA (1986) An air-sea interaction theory for tropical cyclones. Part I: steady-state maintenance. *J Atmos Sci* 43:585–605
- Feng XR, Yin BS, Yang DZ (2016) Development of an unstructured-grid wave-current coupled model and its application. *Ocean Model* 104:213–225
- Sea level station monitoring facility. Accessed at <https://www.ioc-sealevelmonitoring.org> at Flanders Marine Institute (VLIZ) and Intergovernmental Oceanographic Commission (IOC), VLIZ (2023) <https://doi.org/10.14284/482>
- Fringer OB, Gerritsen M, Street RL (2006) An unstructured-grid, finite-volume, nonhydrostatic, parallel coastal ocean simulator. *Ocean Model* 14(3–4):139–173. <https://doi.org/10.1016/j.ocemod.2006.03.006>
- Gray M, Danard MB, Flather R, Henry RF, Murty TS, Venkatesh S, Jarvis C (1984) A preliminary investigation using a Nova Scotia storm surge prediction model. *Atmos Ocean* 22:207–225
- Greenberg DA Mathematical studies of tidal behaviour in the Bay of Fundy. Ms. Rep. Ser. No. 46, Dep. Fish. and Environ., Ottawa (1977) Ont., 127 pp
- Guo H, Yin K, Huang C (2022) Modeling of direct economic losses of Storm Surge disasters based on a Novel hybrid forecasting system. *Front Mar Sci* 8:804541. <https://doi.org/10.3389/fmars.2021.804541>
- Hallegatte S, Green C, Nicholls RJ, Corfee-Morlot J (2013) Future flood losses in major coastal cities. *Nat Clim Change* 3(9):802
- Han X, Sheng JM, Pan XS, Liu SC, Li CH (2019) Study on the refined storm surge numerical model in the Southern Yellow Sea. *Mar FORECASTS* 36(1):52–58. <https://doi.org/10.11737/j.issn.1003-0239.2019.01.006>(in Chinese)
- He L, Li G, Li K, Shu Y (2014) Estimation of regional sea level change in the Pearl River Delta from tide gauge and satellite altimetry data. *Estuar Coast Shelf Sci* 141:69–77
- Henry RF (1982) Automated programming of explicit shallow water models. Part I. Linearized models with linear and quadratic friction. Can. Tech. Rep. Hydrogr. Ocean Sci., No. 3, Inst. of Ocean Sciences, Dep. Fish. and Oceans, Sidney, B.C., 70 pp
- Holland GJ (1980) An analytic model of the wind and pressure profiles in hurricanes. *Mon Wea Rev* 108:1212–1218. [Available online at https://journals.ametsoc.org/view/journals/mwre/108/8/1520-0493_1980_108_1212_aamotw_2_0_co_2.xml]

- Huang Z, Zong Y, Zhang W (2004) Coastal inundation due to sea level rise in the Pearl River Delta, China. *Nat Hazards* 33(2):247–264
- Huang P, Lin II, Chou C et al (2015) Change in ocean subsurface environment to suppress tropical cyclone intensification under global warming. *Nat Commun* 6:7188
- International Monetary Fund (2018) World Economic Outlook Database
- Jelesnianski CP (1972) SPLASH, pt. I, Landfall storms. NOAA Tech Memorandum NWS TDL, 46, 1–52. [Available online at <https://repository.library.noaa.gov/view/noaa/13509>]
- Jelesnianski CP, Chen J, Shaffer WA, Gilad AJ (1984) SLOSH- a hurricane storm surge forecasting model. *Oceans*, pp 314–317. <https://doi.org/10.1109/OCEANS.1984.1152341>
- Jin FF, Boucharel J, Lin II (2014) Eastern Pacific tropical cyclones intensified by El Niño delivery of subsurface ocean heat. *Nature* 516:82–85
- Kobayashi MH, Pereira JMC, Pereira JCF (1999) A conservative finite-volume second-order-accurate projection method on hybrid unstructured grids. *J Comput Phys* 150:40–45. <https://doi.org/10.1006/jcph.1998.6163>
- Kohno N, Dube SK, Entel M, Fakhruddin S, Greenslade D, Leroux M, Rhome J, Thuy NB (2018) Recent progress in storm surge forecasting. *Trop Cyclone Res Rev* 7(2):55–66. <https://doi.org/10.6057/2018TRR02.04>
- Large WG, Pond S (1981) Open ocean momentum flux measurements in moderate to strong winds. *J Phys Oceanogr* 11(3):324–336. [Available online at https://journals.ametsoc.org/view/journals/phoc/11/3/1520-0485_1981_011_0324_oomfmi_2_0_co_2.xml]
- Li L, Yang J, Lin C-Y et al (2018) Field survey of Typhoon Hato (2017) and a comparison with storm surge modeling in Macau. *Natural Hazards and Earth System Sciences*, 18(12), 3167–3178
- Li Ruiyi, Lu QF, Wei M, Wu L, Li RF, Wang SD, Liu H (2023) Dynamic field retrieval and analysis of structural evolution in offshore core area of typhoon higos based on ground-based radar observation. *Remote Sensing* 15(3):809. <https://doi.org/10.3390/rs15030809>
- Liu H, Li J (2010) An improvement in forecasting rapid intensification of Typhoon Sinlaku (2008) using clear-sky full spatial resolution advanced IR soundings. *J Appl Meteorol Climatology* 49(4):821–827. <https://doi.org/10.1175/2009JAMC2374.1>
- Liu S, Tao DD, Zhao K, Minamide M, Zhang FQ (2018) Dynamics and predictability of the rapid intensification of Super Typhoon Usagi (2013). *J Geophys Research: Atmos* 123(14):7462–7481. <https://doi.org/10.1029/2018JD028561>
- Liu Qiuxing D, Jianxi Y, Fujiang et al (2014) A high-resolution typhoon storm surge forecast model covering the whole China's coastal areas and its application. *Acta Oceanol Sin* 36(11):30–37. <https://doi.org/10.3969/j.issn.025.> (in Chinese)
- Lu XQ, Yu H, Ying M, Zhao BK, Zhang S, Lin LM, Bai LN, Wan RJ (2021) Western North Pacific tropical cyclone database created by the China Meteorological Administration. *Adv Atmos Sci* 38(4):690–699. <https://doi.org/10.1007/s00376-020-0211-7>
- Luettich RA, Westerink JJ (2004) Formulation and numerical implementation of the 2D/3D ADCIRC finite element model version 44.XX. pp. 74 [Available online at https://adcirc.org/wp-content/uploads/sites/2255/2018/11/2004_Luettich.pdf]
- Mellor GL, Yamada T (1982) Development of a turbulence closure model for geophysical fluid problem. *Rev Geophys Space Phys* 20:851–875. <https://doi.org/10.1029/RG020i004p00851>
- Muis S, Verlaan M, Winsemius H, Aerts J, Ward P (2016) Global reanalysis of storm surges and extreme sea levels. *Nat Commun* 7:1–11. <https://doi.org/10.1038/ncomms11969>
- Mumaw LM, Ison R, Corney H, Gaskell N, Kelly I (2023) Reframing governance possibilities for urban biodiversity conservation through systemic co-inquiry. *Environ Policy Gov* 1–14. <https://doi.org/10.1002/eet.2047>
- Needham HF, Keim BD, Sathiaraj D (2015) A review of tropical cyclone-generated storm surges: global data sources, observations, and impacts. *Rev Geophys* 53(2):545–591. <https://doi.org/10.1002/2014RG000477>
- Oey LY (2016) Evidence of rising and poleward shift of storm surge in Western North Pacific in recent decades. *J Geophys Res-Oceans* 121:5181–5192. <https://doi.org/10.1002/2016JC011777>
- Passeri DL, Hagen SC, Medeiros SC, Bilskie MV, Alizad K, Wang D (2015) The dynamic effects of sea level rise on low-gradient coastal landscapes: a review. *Earths Future* 3(6):159–181
- Peng SQ, Li YN (2015) A parabolic model of drag coefficient for storm surge simulation in the South China Sea. *Sci Rep* 5:15496. <https://doi.org/10.1038/srep15496>
- Petzelterberger BEM (2000) Coastal development and human activities in NW Germany. In: Pye K, Allen JRL (eds) *Coastal and Estuarine environments: Sedimentology, Geomorphology and Geoarchaeology*, vol 175. Geological Society, London, Special Publication, p 365e376
- Pore NA (1964) The relation of wind and pressure to extratropical storm surges at Atlantic City. *J Appl Meteorol* 3:155–163. [https://doi.org/10.1175/1520-0450\(1964\)003<0155:TROWAP>2.0.CO;2](https://doi.org/10.1175/1520-0450(1964)003<0155:TROWAP>2.0.CO;2)

- Qu Y, Jevrejeva S, Jackson LP, Moore JC (2018) Coastal sea level rise around the China seas. *Glob Planet Change* 172:454–463
- Salmun H, Molod A (2015) The use of a statistical model of storm surge as a bias correction for dynamical surge models and its applicability along the U.S. East Coast. *J Mar Sci Eng* 3:73–86. <https://doi.org/10.3390/jmse3010073>
- Sasaki W, Iizuka S (2007) Sensitivity of model resolution to wave setup calculation. Poster in JCOMM 1st Storm Surge Symposium
- Shen Y, Deng G, Xu Z, Tang J (2019) Effects of sea level rise on storm surge and waves within the Yangtze River Estuary. *Front Earth Sci* 13(2):303–316
- Shi YP, Du Y, Chen ZS, Zhou W (2020) Occurrence and impacts of tropical cyclones over the southern South China Sea. *Int J Climatol* 40(9):4218–4227. <https://doi.org/10.1002/joc.6454>
- Smagorinsky J (1963) General circulation experiments with the primitive equations, I. The basic experiment. *Mon Weather Rev* 91:99–164. [Available online at https://journals.ametsoc.org/view/journals/mwre/91/3/1520-0493_1963_091_0099_gcewtp_2_3_co_2.xml?tab_body=pdf]
- Srивer RL, Huber M (2007) Observational evidence for an ocean heat pump induced by tropical cyclones. *Nature* 447:577–580
- Tadesse M, Wahl T, Cid A (2020) Data-Driven modeling of global storm surges. *Front Mar Sci* 7:260. <https://doi.org/10.3389/fmars.2020.00260>
- Takagi H, Thao ND, Esteban M (2014) Tropical cyclones and storm surges in Southern Vietnam. In: Thao ND, Takagi H, Esteban M (eds) Coastal disasters and climate change in Vietnam: engineering and planning perspectives, 1st edn. Elsevier, pp 3–16
- Tan Y, Zhang X, Xu XL, Huang W (2022) Improvements in the GRAPES-TCM and the forecast performance analysis in 2019. *Front Earth Sci* 16:144–157. <https://doi.org/10.1007/s11707-021-0899-4>
- Velden C, Lewis WE, Bresky W, Stettner D, Daniels J, Wanzong S (2017) Assimilation of high-resolution satellite-derived atmospheric motion vectors: impact on HWRF forecasts of tropical cyclone track and intensity. *Mon Weather Rev* 145(3):1107–1125. <https://doi.org/10.1175/MWR-D-16-0229.1>
- Von Storch H, Woth K (2008) Storm surges, perspectives and options. *Sustain Sci* 3:33e44. <https://doi.org/10.1007/s11625-008-0044-2>
- Weng YH, Zhang FQ (2016) Advances in convection-permitting tropical cyclone analysis and prediction through EnKF assimilation of reconnaissance aircraft observations. *J Meteorol Soc Jpn* 94(4):345–358. <https://doi.org/10.2151/jmsj.2016-018>
- World Bank (2015) East Asia's changing Urban Landscape: measuring a decade of spatial growth. Urban Development Series. World Bank, Washington, DC. <https://doi.org/10.1596/978-1-4648-0363-5>
- Xiong J, Fu CF, Yu FJ, Dong JX (2022) Verification and analysis of numerical forecast of typhoon In-Fa and hurricane Ida storm surge based on ECMWF fine grid wind field. *Mar Forecasts* 39(3):1–9. <https://doi.org/10.11737/j.issn.1003-0239.2022.03.001> (in Chinese)
- Yang Z, Wang T, Voisin N, Copping A (2015) Estuarine response to river flow and sea-level rise under future climate change and human development. *Estuar Coast Shelf Sci* 156:19–30
- Zhang XB (2018) A GRAPES-based mesoscale ensemble prediction system for tropical cyclone forecasting: configuration and performance. *Q J R Meteorol Soc* 144(711):478–498. <https://doi.org/10.1002/qj.3220>
- Zhang Y, Baptista AM (2008) SELFE: a semi-implicit eulerian–lagrangian finite-element model for cross-scale ocean circulation. *Ocean Modell* 21(3–4):71–96
- Zhang YJ, Ye F, Stanev EV, Grashorn S (2016) Seamless cross-scale modeling with SCHISM. *Ocean Model* 102:64–81. <https://doi.org/10.1016/j.ocemod.2016.05.002>
- Zhang L, Fu CF, Dong JX et al (2021) Numerical simulation of storm surge inundation in block scale. *Haiyang Xuebao* 43(10):38–49. <https://doi.org/10.12284/hyxb20211161> (in Chinese)
- Zhong SX, Chen ZT (2015) Improved wind and precipitation forecasts over South China using a modified orographic drag parameterization scheme. *J Meteor Res* 29(1):132–143. <https://doi.org/10.1007/s13351-014-4934-1>
- Zhong SX, Chen ZT, Xu DS et al (2020) A review on GRAPES-TMM operational model system at Guangzhou Regional Meteorological Center. *J Trop Meteorol* 26(4):495–504. <https://doi.org/10.46267/j.10.46267/j.1006-8775.2020.043>
- Zhou L, Chen DK, Lei XT et al (2019) Progress and perspective on interactions between ocean and typhoon (in Chinese). *Chin Sci Bull* 64:60–72. <https://doi.org/10.1360/N972018-00668>

Publisher's note Springer Nature remains neutral with regard to jurisdictional claims in published maps and institutional affiliations.

Springer Nature or its licensor (e.g. a society or other partner) holds exclusive rights to this article under a publishing agreement with the author(s) or other rightsholder(s); author self-archiving of the accepted manuscript version of this article is solely governed by the terms of such publishing agreement and applicable law.